JOURNAL OF MATERIALS SCIENCE 32 (1997) 17–21

Dielectric and field-induced strain behaviour of $(Pb_{1-x}Ba_x)\ ZrO_3$ ceramics

KI HYUN YOON, SOON CHEOL HWANG
Department of Ceramic Engineering, Yonsei University, Seoul 120-749, Korea

DONG HEON KANG
Department of Electronic Materials Engineering, The University of Suwon, Suwon 445-743, Korea

The effects of Ba^{2+} substitution on the dielectric properties and induced strain behaviour of the $(Pb_{1-x}Ba_x)\ ZrO_3$ ceramics ($0.05 \leqslant x \leqslant 0.3$) have been investigated as a function of x. A new phase diagram of the $(Pb_{1-x}Ba_x)\ ZrO_3$ system, indicating the field effect on the phase transition, is also presented. As the Ba^{2+} content increases, the Curie temperature decreases linearly, whereas maximum dielectric constant increases for up to 20 mol % Ba^{2+} addition, and then decreases with further Ba^{2+} addition. Based on the hysteresis loops, the temperature range of the ferroelectric phase as an intermediate phase between the antiferroelectric and paraelectric phases, increases with increasing electric field and Ba^{2+} content. The ferroelectric loops are induced at room temperature for the specimens containing above 10 mol % Ba^{2+} by applying an electric field up to $\sim 25\ kV\,cm^{-1}$. However, for the 5 mol % Ba^{2+}-substituted specimen, no ferroelectric loop is induced, even with applied fields up to $55\ kV\,cm^{-1}$. The phase transition due to electric field and Ba^{2+} addition is also confirmed by the measurement of the field-induced longitudinal strain.

1. Introduction

Since the first characterization of $PbZrO_3$ as antiferroelectric (AFE) by Sawaguchi et al. [1], its dielectric properties, crystal structure and phase diagram have been intensively investigated [2–4]. $PbZrO_3$ has an orthorhombic crystal structure modification of the ABO_3 perovskite type at room temperature, and its dielectric constant shows a sharp maximum at the phase transition from orthorhombic to cubic at the Curie point near 230 °C. Roberts [5] and Shirane *et al.* [6, 7] reported that when Ba^{2+} ions replaced some of the Pb^{2+} ions in $PbZrO_3$ another transition, besides the ordinary Curie point, could be observed at a relatively lower temperature, and that the Curie temperature decreased with increasing Ba^{2+} concentration. The intermediate phase between these two transitions was determined to be ferroelectric (FE) by observation of dielectric hysteresis curves. The phase diagram of the $(Pb_{1-x}Ba_x)\ ZrO_3$ system from the permittivity measurement was presented; Shirane [6] reported that the FE intermediate phase did not appear until the Ba^{2+} concentration reached a threshold value which seemed to be slightly above 5 mol %, and also reported that a forced transition from the AFE phase to the FE one was possible by the application of a strong electric field. On the contrary, Ujma *et al.* [8]recently reported the FE phase existence in $(Pb_{1-x}Ba_x)\ ZrO_3$ containing up to 5 mol % Ba^{2+}, with dielectric properties different from the previous papers [2, 4]. From the results of fully saturated hysteresis loops, a phase diagram different from Shirane's was constructed. These results show that the AFE–FE and FE–PE phase transitions and the basic dielectric properties of $PbZrO_3$ are significantly influenced by the introduction of Ba^{2+} ions and the application of an electric field. However, the field-induced phase transition in $(Pb_{1-x}Ba_x)\ ZrO_3$ with variations of Ba^{2+} content and temperature, has not been reported in detail.

In this study, the dielectric properties and field-induced strain behaviour of $(Pb_{1-x}Ba_x)ZrO_3$ ceramics ($0.05 \leqslant x \leqslant 0.3$) are investigated precisely as a function of x and electric field.

2. Experimental procedure

$(Pb_{1-x}Ba_x)ZrO_3$ ceramics were prepared by the usual ceramic processing technique. Reagent-grade PbO, ZrO_2 and $BaCO_3$ powders were used as the starting materials. The oxides mixed by ball milling for 24 h were calcined at 1000 °C for 1 h. The calcined powders were analysed by X-ray diffractometry (XRD) to confirm complete formation of the perovskite structure. After calcining, the powders were isostatically pressed into pellets at a pressure of 20 000 p.s.i. (10^3 p.s.i. = $6.89\ N\,mm^{-2}$). The pressed pellets were sintered at 1200–1300 °C for 3 h with a heating rate of $300\ °C\,h^{-1}$ in a PbO atmosphere to avoid PbO sublimation. The sintering temperature was experimentally optimized to obtain specimens with a relative density above 96%–97%. Following this, the microstructures of

0022–2461

polished and etched surfaces were examined by scanning electron microscopy (SEM). Specimens for dielectric measurements were prepared from sintered pellets by polishing the faces flat and by firing on silver electrodes at 590 °C for 10 min. Dielectric permittivity and loss were measured using an LCR meter at 1 kHz. In order to investigate temperature and field dependences of the phase transition, *P–E* hysteresis loops were measured using a Sawyer–Tower circuit at 0.1–10 Hz with a temperature control system. Field-induced longitudinal strain curves were measured with an Accumeasure system (M.T.I 1000, USA) at about 50 °C in order to stabilize electrical contact.

3. Results and discussion

XRD patterns of the calcined $(Pb_{1-x}Ba_x)ZrO_3$ powders are shown in Fig. 1. Other than the perovskite phase was not observed for the whole range of compositions. Also the XRD patterns indicate that the replacement of Pb^{2+} by Ba^{2+} ions apparently influenced the orthorhombic $PbZrO_3$ structure. Considering the fact that the peak splitting between (4 0 0) and (0 4 2) vanished above 25 mol % Ba^{2+} substitution, the structure of $(Pb_{1-x}Ba_x)ZrO_3$ changed from orthorhombic to rhombohedral at around $(Pb_{0.75}Ba_{0.25})ZrO_3$ composition, which was confirmed by the lattice constant measurement of this system. Additionally, the symmetry of $(Pb_{1-x}Ba_x)ZrO_3$ structure is thought to be increased by the substitution of Ba^{2+} ions with larger ionic radius (0.143 nm) with Pb^{2+} (0.132 nm), which may be explained by the effect of cubic $BaZrO_3$. A similar result was reported by Shirane and Hoshino [7]

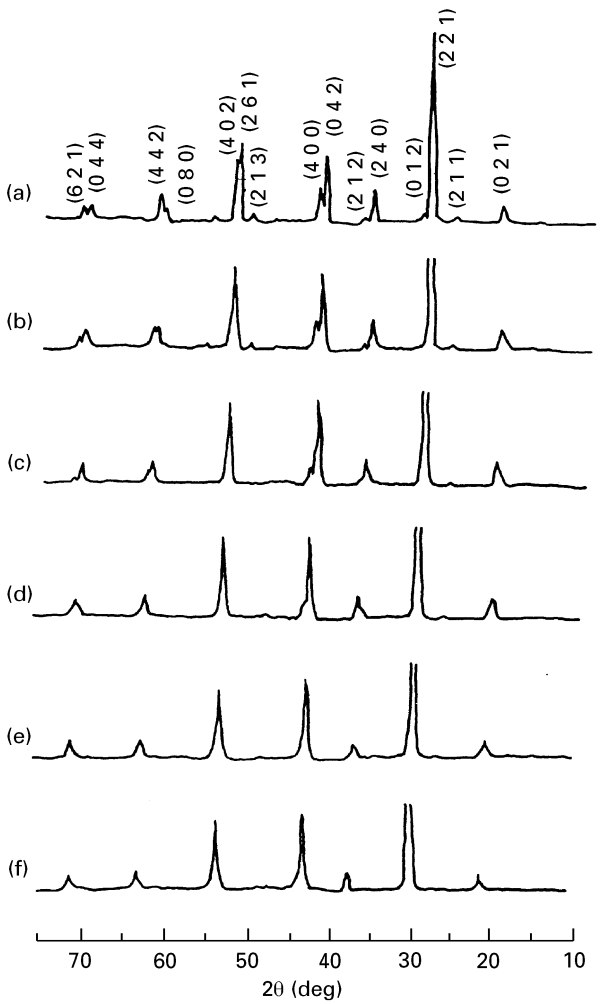

Figure 1 XRD patterns of $(Pb_{1-x}Ba_x)ZrO_3$ powders calcined at 1000 °C for 1 h. (a) $x = 0.05$, (b) $x = 0.1$, (c) $x = 0.15$, (d) $x = 0.2$, (e) $x = 0.25$, and (f) $x = 0.3$.

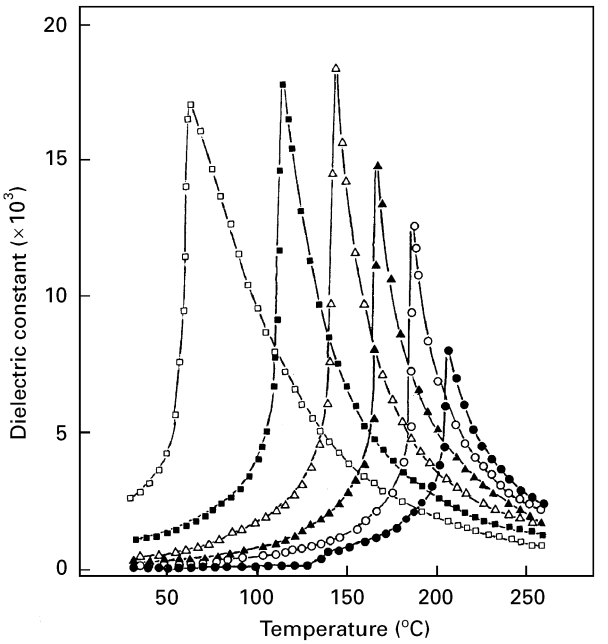

Figure 2 Dielectric constant versus temperature for $(Pb_{1-x}Ba_x)ZrO_3$ specimens as a function of x. $x =$ (●) 0.05, (○) 0.1, (▲) 0.15, (△) 0.2, (■) 0.25, and (□) 0.3.

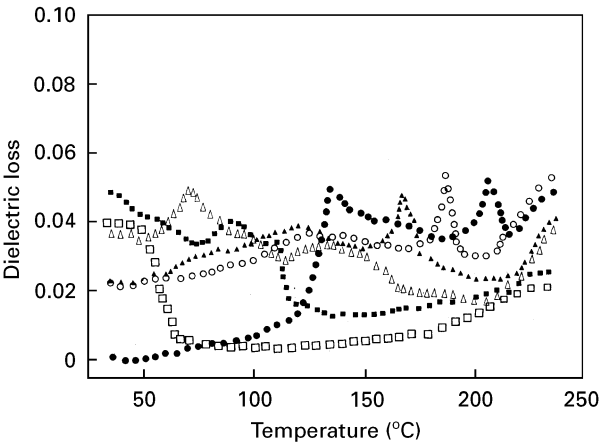

Figure 3 Dielectric loss versus temperature for $(Pb_{1-x}Ba_x)ZrO_3$ specimens as a function of x. $x =$ (●) 0.05, (○) 0.1, (▲) 0.15, (△) 0.2, (■) 0.25, and (□) 0.3.

The dielectric constant and loss versus temperature curves of the $(Pb_{1-x}Ba_x)ZrO_3$ specimens containing various amounts of Ba^{2+} ($0.05 \leqslant x \leqslant 0.3$) are shown in Figs 2 and 3. As the amount Ba^{2+} increased up to 20 mol %, the maximum dielectric constant increased rapidly. This increase in dielectric constant is thought to be related to the change of $(Pb_{1-x}Ba_x)ZrO_3$ structure. The substitution of larger Ba^{2+} ions with Pb^{2+} sites, which implies the transition of $(Pb_{1-x}Ba_x)ZrO_3$ structure from orthorhombic to rhombohedral as

shown in Fig. 1, may facilitate the parallel displacement along a [1 1 1] direction and the associated displacements of three oxygen ions in $(Pb_{1-x}Ba_x)ZrO_3$ structure, resulting in an improvement of ferroelectricity. The presence of a polar axis in the [1 1 1] direction has been reported for a ferroelectric rhombohedral structure [7]. However, above 25 mol % Ba^{2+} composition, a slight decrease in the maximum dielectric constant was observed. As shown in Fig. 2, the Curie temperature shifted to a lower temperature linearly, which may be explained by the increase of symmetry in $(Pb_{1-x}Ba_x)ZrO_3$ structure with increasing Ba^{2+} ions as previously mentioned. These results are similar to those reported in earlier papers [5, 8]. However, in this study, the specimens exhibited a much higher dielectric constant and lower loss, probably due to better conditions for the sintering process. Also, the dielectric constant–temperature curve in Fig. 2 implies that the well-sintered $(Pb_{1-x}Ba_x)ZrO_3$ specimens lowered the Curie temperatures by about 20–30 °C compared to those of other reports for same composition [6, 8], indicating that more homogeneous solid solutions were prepared in the study [9]. The curve for $(Pb_{0.95}Ba_{0.05})ZrO_3$ in Fig. 2 shows another small anomaly at about 145 °C besides a sharp maximum at 205 °C. Shirane [6] reported it as a transition temperature from an antiferroelectric (AFE) phase to a ferroelectric (FE) one. The increase in the amount of Ba^{2+} is accompanied by a decrease in the transition temperatures at which the small anomalies are observed. For the 30 mol % Ba^{2+}-substituted specimen, this small anomaly was not observed, even at room temperature, indicating that the ferroelectric phase is stable at room temperature.

In this study the P–E hysteresis loops were measured under various electric fields in order to ascertain the field effect on a phase transition. The applied voltage was varied from 5 kV cm^{-1} to the saturation field and the P–E hysteresis loops were measured at each field as a function of temperature. The choice of the lower field as 5 kV cm^{-1} may be expected to exclude the influence of forced phase transition by an electric field in the system. Figs 4 and 5 show the temperature dependence of the *P–E* hysteresis loops for the $(Pb_{0.95}Ba_{0.05})ZrO_3$ and $(Pb_{0.7}Ba_{0.3})ZrO_3$ ceramics under 5 kV cm^{-1}, respectively. For the composition of $(Pb_{0.95}Ba_{0.05})ZrO_3$, the P–E hysteresis loop changes its shape from nearly linear to broad with increasing temperature. A ferroelectric hysteresis gradually appeared at temperatures higher than about 145 °C and then became linear at the Curie temperature, suggesting that the ferroelectric phase is stable in the temperature range from 145–205 °C, whereas, for the composition of $(Pb_{0.7}Ba_{0.3})ZrO_3$ shown in Fig. 5, a typical ferroelectric hysteresis loop appeared at room temperature and then also became linear at above ~70 °C. The critical value of temperature at which the intermediate phase began to appear was estimated for other compositions by similar measurements. Additionally, as the biasing field increased from 5 kV cm^{-1} to 30 kV cm^{-1}, hysteresis loops were investigated with variations of Ba^{2+} content and temperature. For all specimens, the AFE–FE transition

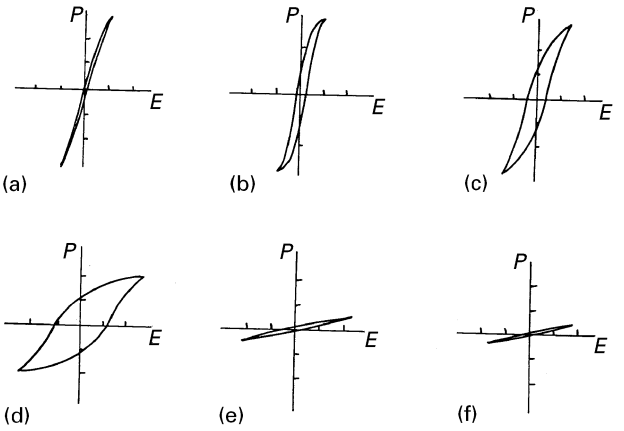

Figure 4 *P* versus *E* hysteresis loops for $(Pb_{0.95}Ba_{0.05})ZrO_3$ specimens at $E_{max} = 5$ kV cm^{-1}. (a) 210 °C, (b) 205 °C, (c) 170 °C, (d) 145 °C, (e) 140 °C, and (f) 30 °C. $P = 10$ μC cm^{-2} per div.

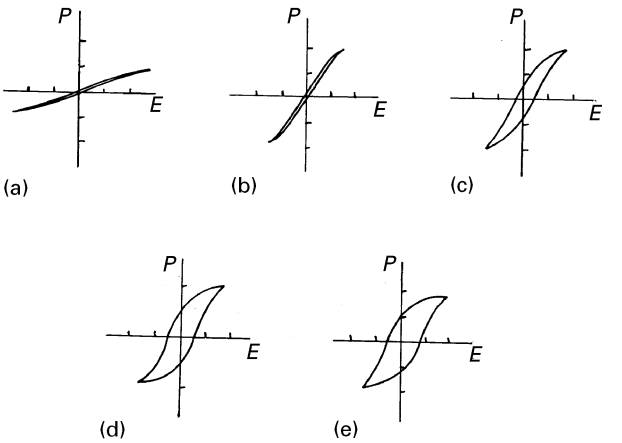

Figure 5 *P* versus *E* hysteresis loops for $(Pb_{0.7}Ba_{0.3})ZrO_3$ specimens at $E_{max} = 5$ kV cm^{-1}. (a) 80 °C, (b) 63 °C, (c) 60 °C, (d) 50 °C, and (e) 30 °C. $P = 10$ μC cm^{-2} per div.

temperatures decreased and the FE–PE transition temperatures slightly increased with increasing electric field. At room temperature, the phase transition from AFE to FE was easily forced under < 25 kV cm^{-1} for the specimens containing 10–30 mol % Ba^{2+}. For $(Pb_{0.95}Ba_{0.05})ZrO_3$, however, the P–E diagram exhibits a typical antiferroelectric hysteresis loop in spite of the application of up to 55 kV cm^{-1}. Upon increasing the temperature up to ~125 °C, the ferroelectric hysteresis loop was induced under 25 kV cm^{-1} for the $(Pb_{0.95}Ba_{0.05})ZrO_3$ specimen. The AFE–FE phase transition for $(Pb_{0.95}Ba_{0.05})ZrO_3$ has been reported by Ujma *et al.* [8]under 5 kV cm^{-1} at ~140 °C. Also, Fesenko *et al.* [10]reported that the phase transition from AFE to FE in single-crystal $PbZrO_3$ could be observed by the application of strong fields as high as 200 kV cm^{-1} and that the level of bias could be reduced with increasing temperature.

Fig. 6 shows the P–E hysteresis loops of the $(Pb_{1-x}Ba_x)ZrO_3$ specimens under saturation field at room temperature. As mentioned previously, the typical ferroelectric hysteresis loops were observed at all compositions except for the $(Pb_{0.95}Ba_{0.05})ZrO_3$ specimen. The increase in Ba^{2+} content resulted in a decrease in both the saturation field and coercive field,

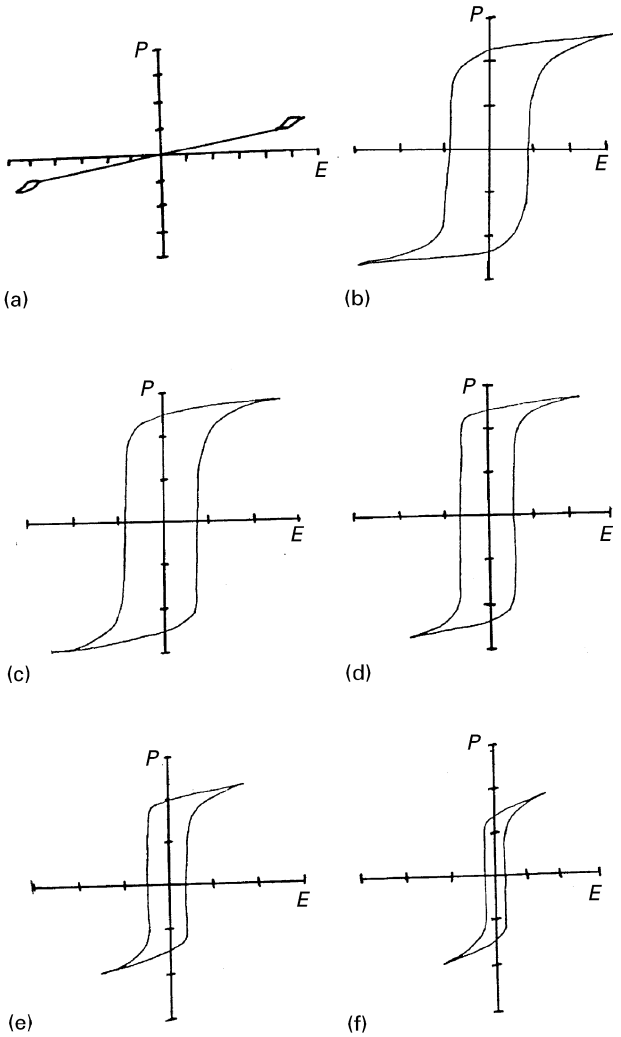

Figure 6 *P* versus *E* hysteresis loops for $(Pb_{1-x}Ba_x)\ ZrO_3$ specimens as a function of *x*. (a) $x = 0.05$, (b) $x = 0.1$, (c) $x = 0.15$, (d) $x = 0.2$, (e) $x = 0.25$, and (f) $x = 0.3$. (g) $E = 10\ kV\,cm^{-1}$ per div., $P = 2\ \mu C\,cm^{-2}$ per div., (b.f) $E = 10\ kV\,cm^{-1}$ per div., $P = 10\ \mu C\,cm^{-2}$ per div.

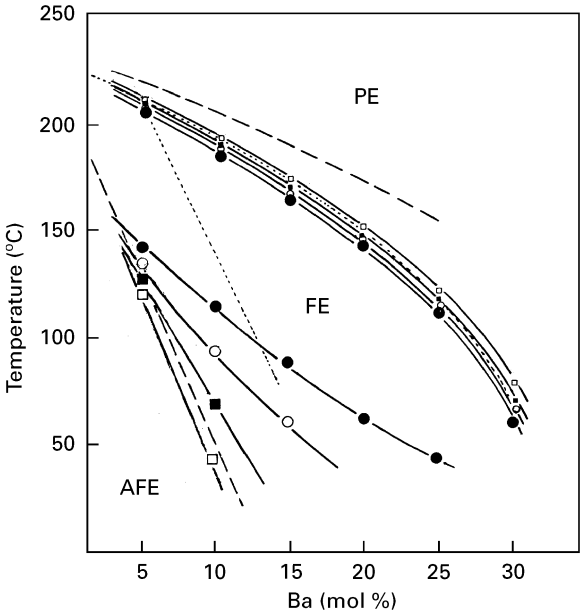

Figure 7 Phase diagram of the $(Pb_{1-x}Ba_x)ZrO_3$ system as a function of applied field: (●) $5\ kV\,cm^{-1}$, (○) $7\ kV\,cm^{-1}$, (■) $10\ kV\,cm^{-1}$, (□) $25\ kV\,cm^{-1}$. (- - -) from Ujma *et al.* [8] (…) from Shirane [6].

suggesting that the stable ferroelectric phase was easily induced by the substitution of Ba^{2+} into Pb^{2+} sites. Also Figs 2 and 6 indicate that the peak composition between remnant polarization, P_r, and dielectric constant, ε_r is apparently different. The maximum P_r at the 10–15 mol % Ba^{2+} composition is explained by the fact that the phase transition could be induced for the compositions with relatively lower Ba^{2+} content due to the application of saturation field, whereas further addition of Ba^{2+} exhibits the degraded P_r despite the stable ferroelectric phase, which is probably related with a lower polarizability of Ba^{2+} compared to that of Pb^{2+}.

Based on the results of hysteresis loops measurement with the variations of electric field and temperature, the phase diagram for the $(Pb_{1-x}Ba_x)\ ZrO_3$ system was constructed as shown in Fig. 7. The transition temperatures obtained from *P–E* hysteresis loops under the lower field as $5\ kV\,cm^{-1}$ agree well with those in ε_r versus *T* as shown in Fig. 2. With increasing electric field, the FE–PE phase transition line slightly increases, probably due to the thermal motion at a relatively higher temperature required to destroy the enhanced polarization. However, the application of electric field reduces the AFE–FE phase transition temperature, which may be associated with a possible rotation of dipole moment of ceramics in the same direction with increasing electric field [11]. Furthermore, the phase diagram apparently shows that as Ba^{2+} content decreases, the temperature dependence on the phase transitions is more effective than that of the electric field and also that the temperature range of the ferroelectric phase is enlarged with increasing biasing field and Ba^{2+} content. Such forced-phase transition may be explained by the fact that the free energy of the ferroelectric phase easily becomes lower than those of the antiferroelectric and paraelectric ones, either by the application of a electric field or by the substitution of Ba^{2+} ions into Pb^{2+} sites [7]. Also Fig. 7 includes the phase diagrams of the $(Pb_{1-x}Ba_x)ZrO_3$ system reported by Shirane [6]and Ujma *et al.* [8]which were determined by the dielectric measurement under no bias and by *P–E* hysteresis loops under $5\ kV\,cm^{-1}$, respectively. The FE–PE transition line of this study is similar to that of Shirane [6]. In particular, when the field strength exceeded $25\ kV\,cm^{-1}$, an FE–PE transition line, lower by $\sim 30\ ^\circ C$ than that of Ujma *et al.*, was obtained as shown in Fig. 7. However, in the case of AFE–FE transition, the transition line is quite different from that of Shirane [6]. The transition lines of the $(Pb_{1-x}Ba_x)ZrO_3$ system obtained with and without electric field in this study are thought to be more reasonable compared to the Shirane which was obtained only without a field [6]

Fig. 8 shows the field-induced longitudinal strain curves as a function of Ba^{2+} content. For the 10 mol % Ba^{2+}-substituted specimen, the initial state of strain is almost zero. Application of an electric field above $15\ kV\,cm^{-1}$ leads to an increase in the level of strain, suggesting the forced transition from an antifer-

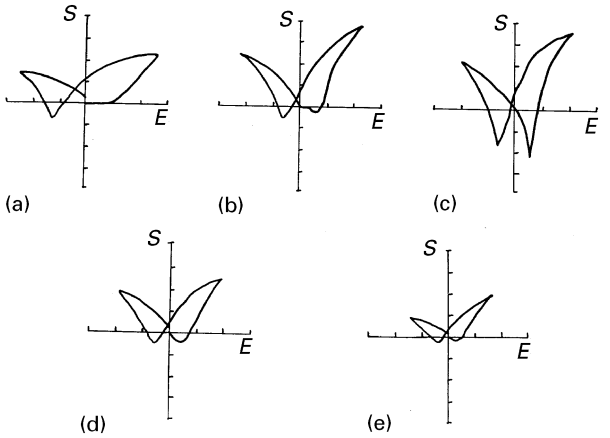

Figure 8 Longitudinal strain versus electric field for $(Pb_{1-x}Ba_x)ZrO_3$ specimens as a function of x. (a) $x = 0.1$, (b) $x = 0.15$, (c) $x = 0.2$, (d) $x = 0.25$, and (e) $x = 0.3$. $E = 15\,kV\,cm^{-1}$ per div., $S = 0.5 \times 10^{-3}$ per div.

roelectric phase to a ferroelectric one. With increasing Ba^{2+} concentration, this threshold field decreased, and when the Ba^{2+} content exceeded 20 mol %, the field-induced strain curve exhibited a typical ferroelectric butterfly curve. But it is changed into a soft type above 25 mol % Ba^{2+} addition, which may be due to the degraded piezoeffect [12]. Based on the fact that the strain in ceramics is due to the superimposition of complicated piezostriction and electrostriction [13], the piezoelectric strain coefficient was estimated from the curves in Fig. 7. For the 20 mol % Ba^{2+} and 30 mol % Ba^{2+}-substituted specimens, the piezoelectric strain coefficients were 750×10^{-12} and $540 \times 10^{-12}\,m\,V^{-1}$, respectively.

4. Conclusion

The maximum dielectric constant of $(Pb_{1-x}Ba_x)ZrO_3$ ceramics increased with increasing Ba^{2+} up to 20 mol %, and then decreased slightly above it. Based on the hysteresis loops, the temperature range of the ferroelectric phase between the antiferroelectric and paraelectric phases was enlarged with increasing electric field and Ba^{2+} content. The fields required to induce the ferroelectric phase decreased with increasing Ba^{2+} content. Compared with the fact that the ferroelectric phase of the $(Pb_{0.9}Ba_{0.1})ZrO_3$ was obtained by applying $25\,kV\,cm^{-1}$ at room temperature, the ferroelectric loop was not induced, even by applying $55\,kV\,cm^{-1}$ for the 5 mol % Ba^{2+}-substituted specimen. The field-induced strain behaviour exhibited strain-curve shapes varying from antiferroelectric to ferroelectric type with increasing electric field and the threshold fields decreased with increasing Ba^{2+} content. The highest levels of strain ($\sim 2.8 \times 10^{-3}$) and remnant polarization ($\sim 25\,\mu C\,cm^{-2}$) were obtained for the 20 mol % Ba^{2+}-substituted specimen.

Acknowledgement

This work was supported by the Center for Interface Science and Engineering of Materials of the KOSEF.

References

1. E. SAWAGUCHI, H. MANIWA and S. HOSHINO, *Phys. Rev.* **83** (1951) 1078.
2. S. FUSHIMI and T. IKEDA, *J. Am. Ceram. Soc.* **50** (1967) 129.
3. F. JONA and G. SHIRANE, *Phys. Rev.* **105** (1957) 849.
4. B. A. SCOTT and G. BURNS, *J. Am. Ceram. Soc.* **55** (1972) 331.
5. S. ROBERTS, *ibid.* **33** (1950) 63.
6. G. SHIRANE, *Phys. Rev.* **86** (1952) 219.
7. G. SHIRANE and S. HOSHINO, *Acta Crystallogr.* **7** (1954) 203.
8. Z. UJMA, J. HANDEREK, M. PAWELEZYK and D. DMYTROW, *Ferroelectrics* **129** (1992) 127.
9. S. NOMURA, *J. Phys. Soc. Jpn* **11** (1956) 9.
10. O. E. FESENKO, R. V. KOLESOVA and YU G. SINDEYEV, *Ferroelectrics* **20** (1978) 177.
11. I. S. ZHELUDEV, "Physics of Crystalline Dielectrics", Vol. 1 (Plenum Press, New York, 1971) pp. 328–31.
12. A. HAGIMURA, M. NAKAJIMA, K. MIYATA and K. UCHINO, in "Proceedings of the 7th International Symposium on Applications of Ferroelectrics", edited by S. B. Knupdnidhi and S. K. Kuntz (IEEE Service Center, Piscataway, N.J., USA.) 1990, pp. 185–188, Urbana-Champaign, June (1990) p. 6.
13. Y. MASUDA, *Jpn J. Appl. Phys.* **33** (1994) 5549.

Received 19 January
and accepted 8 May 1996